Examination methods for the physicochemical properties of synthetic membranes

Wolfgang Pusch

Max-Planck-Institut für Biophysik, Kennedy-Allee 70, D-6000 Frankfurt am Main, Bundesrepublik Deutschland

ABSTRACT

Methods for the examination of the physico-chemical properties of synthetic membranes are discussed starting with the determination of membrane pore structure and organization. Subsequently, the determination of equilibrium (e.g. water content, fixed charge concentration) and transport parameters of synthetic membranes is outlined. Using the phenomenological relationships of the thermodynamics of irreversible processes, the hydrodynamic and osmotic permeability, the reflection coefficient, and the asymptotic solute (salt) rejection can be obtained from dialysis and hyperfiltration experiments. The experimental set-ups for both dialysis and hyperfiltration experiments are described.

INTRODUCTION

The broad application of synthetic membranes in technical separation processes, electrochemistry, chloride-alkali electrolysis, and in medicine, for instance, requires a large variety of membranes. In order to select the most appropriate membrane for a specific separation process, it is thus necessary to know the physico-chemical properties of the commercially available synthetic membranes such as their pore size distribution, water content and sorption isotherm, fixed charge concentration, solute partition coefficients, transport parameters as well as to characterize their chemical and mechanical stability. The evaluation of the physico-chemical properties of synthetic membranes requires at first a classification of membranes according to their pore structure (coarse porous, fine porous, dense) and according to their organization (homogeneous, asymmetric, composite). This classification can be obtained only by electron microscopic investigation of appropriate membrane samples. Using transmission and scanning electron micrographs of the surfaces and cross-sections of typical membranes, the pore structure and organization of synthetic membranes is discussed and correlated with their transport and separation properties.

Coarse porous membranes, which are generally applied in micro- and ultrafiltration to concentrate high molecular weight substances and to separate high from low molecular weight substances (e.g. polymers from electrolytes), exhibit pores under the electron microscope with diameters ranging from about 50 Å up to several μm (1 to maximum 5 μm). Although there exists a correlation between the pore size and the molecular size of molecules which can still permeate a membrane with a distinct average pore size, this correlation is very limited since interactions of molecules with the membrane matrix (pore walls of the membrane) play a much greater role for the permeation of a molecule than its molecular size. This was demonstrated by electron microscopic pictures of NUCLEPORE membranes which were used for the filtration of styrene particles and erythrocytes [1]. As a consequence of strong interactions between the styrene particles and the membrane pore walls, the particles do not permeate the membrane although their diameters are only about one tenth of the membrane pore diameter.

In contrast to coarse porous membranes, fine porous membranes do not exhibit pores under the electron microscope. Therefore, one cannot distinguish between fine porous and dense membranes by electron microscopic investigations. To some extent, a differentiation is possible only by indirect methods such as fluid permeation, especially gas permeation measurements. Measuring, for instance, the gas permeation of synthetic membranes as a function of the gas feed pressure over a broad pressure range (0.1 bar up to 50 or even 100 bar), renders possible to some degree the estimation of an average pore size provided appropriate membrane model relationships are being employed [2].

In general, however, an average pore diameter of a fine porous membrane does not supply a very relevant figure since it does not adequately characterize the permeation and separation properties of the corresponding membrane. Only in the case of gas separation, it might occasionally be useful to have information on the existence of micropores within a membrane since convective pore-flow through such pores will diminish the separation performance of the membrane for gas mixtures. A full characterization of synthetic membranes, employed for the separation of solutes from each other and of solutes from solvents, requires the determination of transport parameters and solute partition coefficients. Solute partition coefficients are equilibrium parameters of the membrane. In case of homogeneous membranes, they can be obtained by equilibrating appropriate membrane samples with solutions of different solute concen-

trations and, subsequently, measuring the uptake of the solute by the membrane as a function of solute concentration. On the other hand, it is nearly impossible to determine solute partition coefficients of asymmetric and composite membranes in the same way since one can obtain only the solute partition coefficients of the entire membrane and not those of the active layer of such membranes which are the solely relevant ones. Transport parameters are obtained from appropriate dialysis-osmosis and hyperfiltration (reverse osmosis) experiments measuring the solvent flux as a function of the pressure and osmotic pressure difference and the solute flux as a function of the concentration difference (equivalent to an osmotic pressure difference) across the membrane. The transport coefficients can then be correlated with the separation performance of the membrane. Table 1 summarizes physico-chemical properties of synthetic membranes which are of great interest (e.g. membrane morphology and organization; mechanical and chemical stability; equilibrium properties; transport properties).

TABLE 1

| PHYSICO-CHEMICAL PROPERTIES OF SYNTHETIC MEMBRANES |
| --- |
| MEMBRANE MORPHOLOGY AND ORGANIZATION
(crystalline, amorphous, glassy, rubbery)
(coarse porous, fine porous, dense = pore free)
(homogeneous, asymmetric, composite) |
| MECHANICAL AND CHEMICAL STABILITY
(pressure resistance)
(resistivity towards chemicals, especially pH, O_2, and Cl_2) |
| EQUILIBRIUM PROPERTIES
(sorption isotherms, fixed charge concentration)
(free and/or bound water) |
| TRANSPORT PROPERTIES
(convection, Fickian and/or pressure diffusion)
(free or hindered diffusion) |

ELECTRON MICROGRAPHS OF MEMBRANES

Exhaustive information on the membrane morphology and organization can be obtained only by electron microscopic investigations of appropriate membrane samples. Scanning (SEM) and transmission (TEM) electron microscopic pictures of typical membranes ar exhibited in Figures 1 to 5. Figures 1a+b show top views of coarse porous membrane filters made from cellulose (1a) and cellulose nitrate (CN; 1b). Further coarse porous membranes are exhibited in Figures 2a-d. There are two kinds of coarse porous membranes: one group has a rather broad pore size distribution (Fig. 2a+b, "sponge structure") whereas the other group has pores of nearly uniform diameter (narrow pore size distribution; Fig. 2c-d, "sieve structure").

The production of membranes with uniform pores originated from the assumption that ultrafilters act like sieves and thus separate molecules according to their size. Thus, many attempts were made to fractionate polymers according to their molecular size using coarse porous membranes with more or less uniform pore diameters. However, Ferry [3] had pointed out already in his review article on ultrafiltration that factors completely different from the molecular size must govern the permeation of molecules through membranes. This is illustrated by SEMs of Nuclepore filters (Fig. 3) which were used for the filtration of polystyrene dispersions. The diameters of the polystyrene particles are clearly much smaller than the pore diameters of the membranes used (≈ 1:10). Nevertheless, the polystyrene particles are nearly completely rejected as they adhere to the pore walls and thus the pores become progressively blocked.

In contrast to coarse porous membranes, fine porous membranes do not exhibit pores under the electron microscope. Cross-sections of typical fine porous membranes are reproduced in Figures 4a-d where cross-sections of cuprophane, cellophane, polycarbonate, and polyacrylonitrile membranes are shown. These membranes are mainly used for dialysis and hemodialysis (artificial kidney). The cuprophane and cellophane membranes are not completely homogeneous but rather possess surface layers clearly differing in structure from the internal homogeneous membrane matrix. Cellulose membranes apparently consist of a fine porous matrix located between two dense (non-porous) surfaces of ca. 1,000 to 3,000 Å thickness.

Figures 5a-d show SEMs of cross-sections of typical asymmetric and composite membranes. All these membranes consist of an extremely thin film (active layer) on top of a more or less porous supporting framework (matrix). In the case of asymmetric membranes, the porosity of the supporting matrix increases across the membrane from top to bottom. The pore diameters, the shape of the pores, and the porosity of the supporting framework can be varied within certain limits by adjusting the composition of the casting solution and conditions of membrane fabrication.
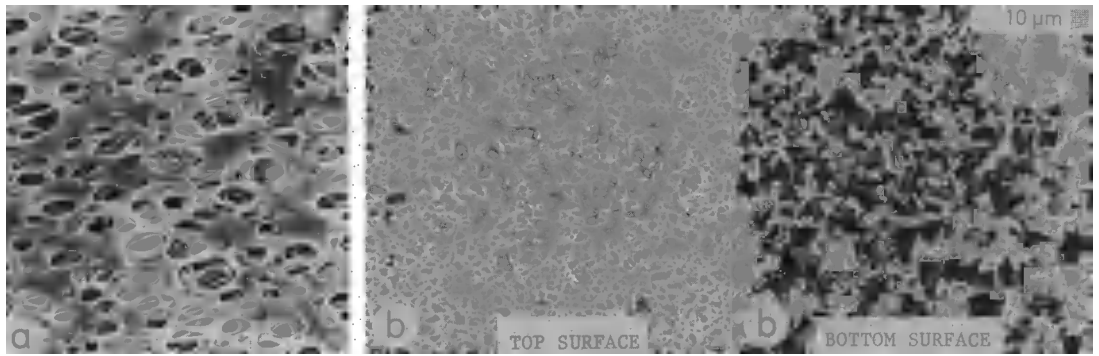
Figures 1a+b: Top views of membrane filters made from cellulose (a; Gelman cellulose-α-450) and from cellulose nitrate (b, Sartorius GmbH); magnification: 3,000 x [1].
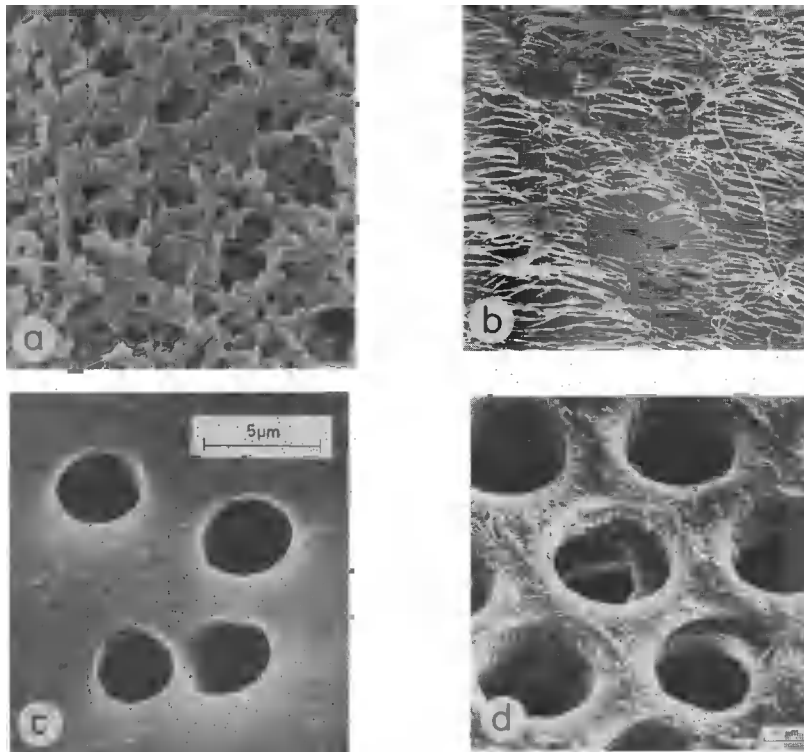
Figures 2a-d: SEMs of top view of Nylon (a; AMF Zetapore), polypropylene (b; Celgard 2400), polycarbonate (c; Nuclepore), and oriented gel membrane (d; Thiele membrane) [1].
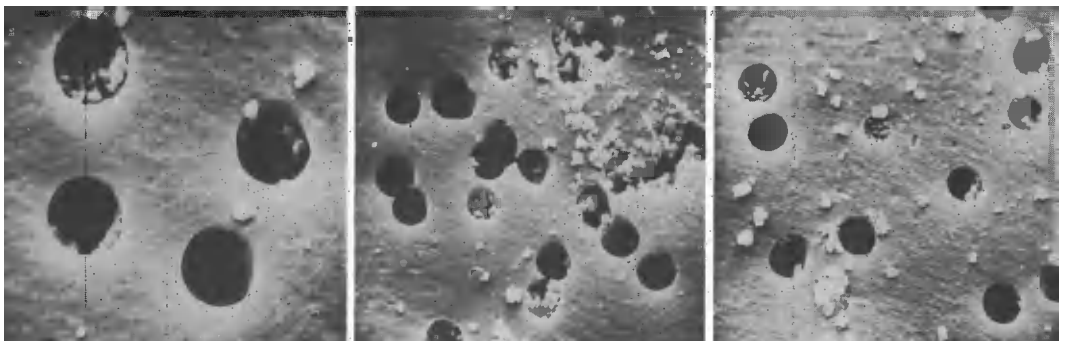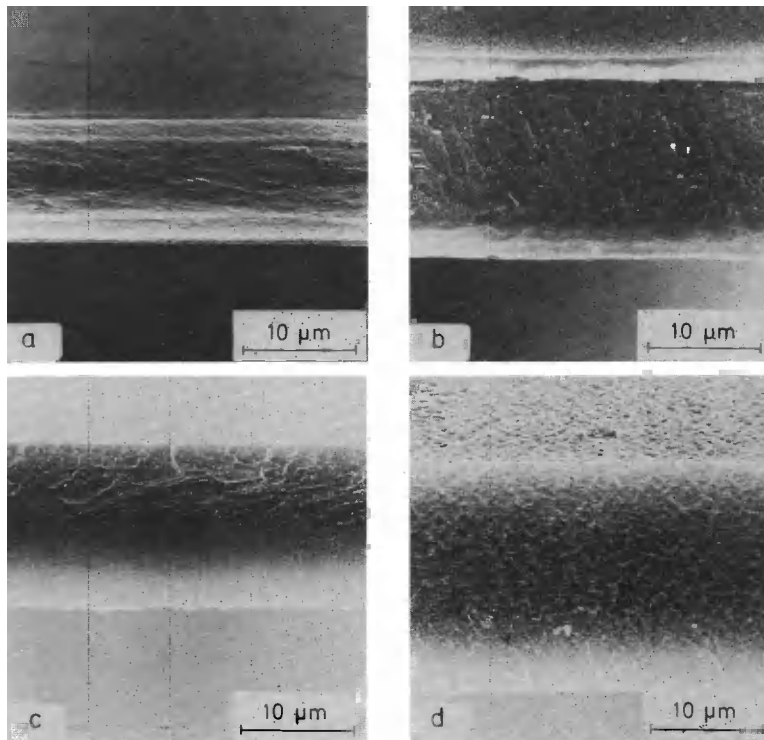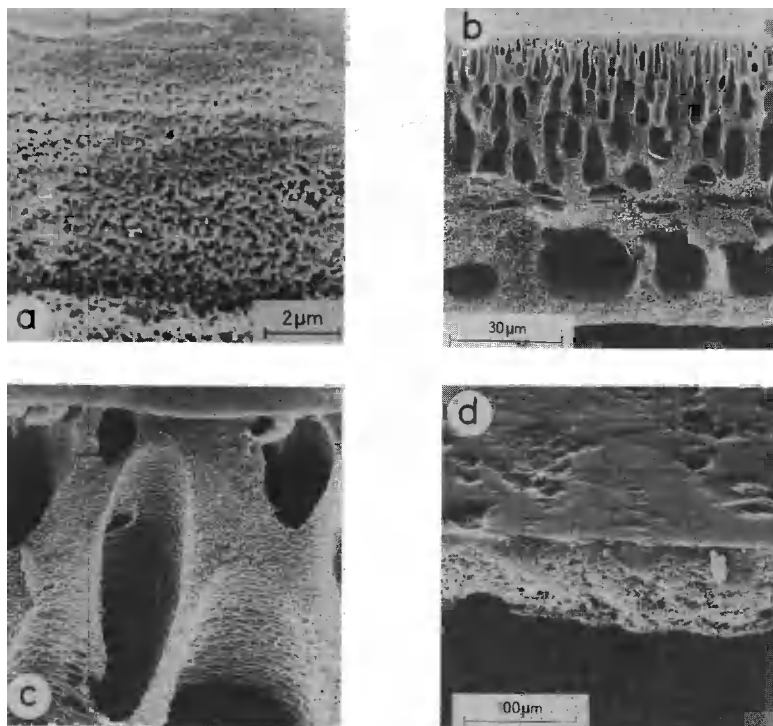

Figure 3: SEMs of top view of Nuclepore filters used for the filtration of polystyrene particles [4].

Figures 4a-d: SEMs of cross-sectional view (with a partial top view of one surface) of a cuprophane (a), a Nadir (b), a polyacrylonitrile (c), and a polycarbonate (d) membrane [1].


Figures 5a-d: SEMs of cross-sections of an asymmetric CA (a), PA (b), PS (c), and a composite RC-100 membrane where the latter one is manufactured by UOP, San Diego, California; the supporting layer is made from PS [1].

EXPERIMENTAL DETERMINATION OF TYPICAL MEMBRANE PARAMETERS

Equilibrium membrane properties

Synthetic membranes are characterized by equilibrium and transport parameters in order to gain a deeper insight into the physico-chemical origin of transport phenomena and possibly relate them to the membrane structure. Among others, the equilibrium properties are the water content, the solute partition coefficients, the fixed charge concentration,. as well as the kind of fixed charge groups and the swelling behavior of the membrane. It is, therefore, absolutely necessary to determine these equilibrium properties if a membrane is to be used for transport measurements.

Determination of membrane water content. In general, the water content of a membrane depends on the water vapor pressure of the surroundings. Measuring the water content of a membrane as a function of water vapor pressure at a constant temperature yields the water sorption isotherm of this membrane. As discussed by several authors [5-7], the pore size distribution within the membrane can be evaluated from the water sorption isotherm applying an appropriate membrane model. Measuring, in addition, the water sorption isotherm at different temperatures renders possible the evaluation of the thermodynamic functions – partial enthalpy, $\Delta \bar{H}_w$, Gibbs free energy, $\Delta \bar{G}_w$, and partial entropy, $\Delta \bar{S}_w$, of water sorption where the reference state is that of bulk water at saturation vapor pressure, $p_{vo}(T)$. Water sorption isotherm measurements might be completed by the determination of the melting behavior of water within a membrane and thus by the evaluation of the partial heat capacity of that water [5,8]. Typical thermodynamic functions of water sorption and the partial heat capacity of water within a membrane are reproduced in Figures 6a+b. As can be seen from Figure 6a, the partial enthalpy and entropy of water sorption, obtained with a homogeneous CA K-700 membrane, are negative. Since the reference state is bulk water at saturation vapor pressure, the small negative value of $\Delta \bar{H}_w$ means that the differential heat of water sorption is about 1 kcal/mol more negative than the heat of condensation of bulk water. Using the thermodynamic potentials of water sorption and the partial heat capacity, information can be obtained about the water structure within a membrane by applying, in addition, appropriate sorption isotherm relationships [9-11]. Knowledge of the pore size distribution and the water structure in a membrane might contribute to the understanding of the transport mechanisms of solute and solvent. Thus, it is possible to classify a special membrane resembling a solution-diffusion, a fine-porous, or a coarse-porous membrane. It would be beyond the scope of this paper to discuss all the details of water sorption measurements. In case of most transport measurements, only the membrane water content at saturation is needed, and that mostly as a function of solute concentration c_s.
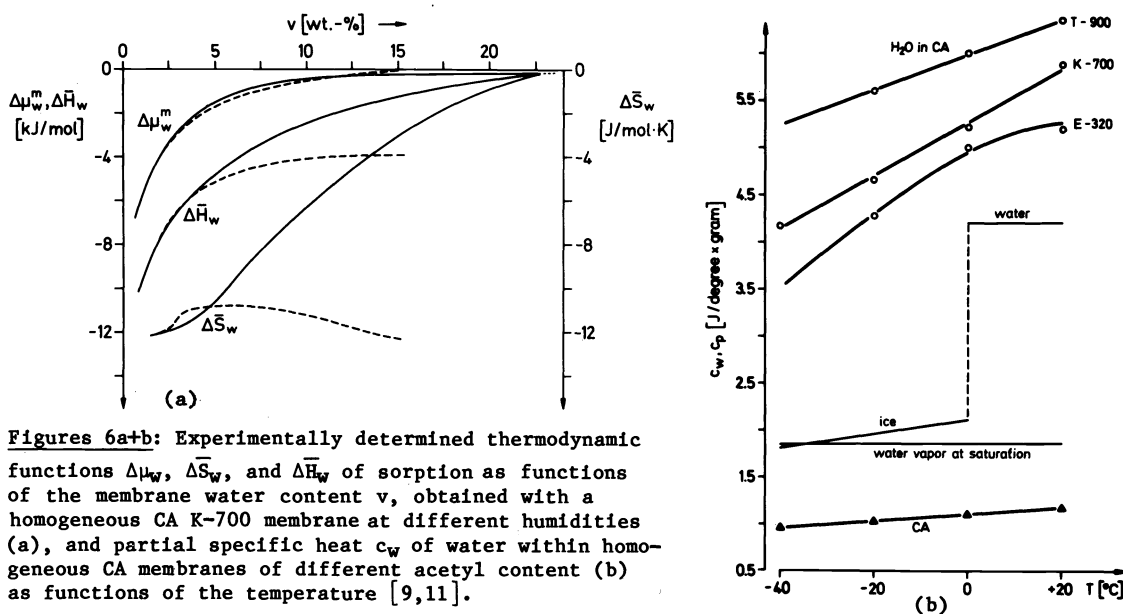
Figures 6a+b: Experimentally determined thermodynamic functions $\Delta \bar{\mu}_w$, $\Delta \bar{S}_w$, and $\Delta \bar{H}_w$ of sorption as functions of the membrane water content v, obtained with a homogeneous CA K-700 membrane at different humidities (a), and partial specific heat c_w of water within homogeneous CA membranes of different acetyl content (b) as functions of the temperature [9,11].

Fixed charge concentration and exchange isotherm. As a consequence of the electroneutrality condition within the membrane, the counterion concentration within an ion-exchange membrane is always larger than the coion concentration. The difference in equivalence balances the fixed charges of the membrane ($C_X \neq 0$). Measuring the salt uptake of an ion-exchange membrane, possessing a constant fixed charge concentration (strong ion-exchange membrane), the anion and cation concentrations within the membrane must be determined as a function of the external salt concentration. The coion concentration is then equal to the salt concentration within the membrane and yields the salt partition coefficient $K_s = K_{co} = C_{co}/\nu_{co}c_s$ where ν_{co} is the stoichiometric number of the coion in the corresponding salt, and c_s is the external salt concentration. The ratio of the counterion concentration within the membrane to the

counterion concentration of the external solution, $C_g/\nu_g c_s$, yields, on the other hand, the counterion partition coefficient, $K_g = C_g/\nu_g c_s$, where ν_g denotes the stoichiometric number of the counterion in the corresponding salt (g = Gegenion). With increasing salt concentration of the external solution, $c_s \to \infty$, the counterion concentration within the membrane approximates the coion concentration and thus K_g approaches the value of $K_s = K_{co}$ at external salt concentrations $c_s \gg C_X$. On the other hand, if the external salt concentration approaches zero, $c_s \to 0$, the coion concentration within the membrane approaches zero as well, whereas the counterion concentration approaches the fixed charge concentration, $C_g \to C_X$ at $c_s \to 0$. Therefore, the salt partition coefficient approaches also zero at $c_s \to 0$ whereas K_g tends to infinity as illustrated in Figure 7. In addition, plotting the counterion concentration itself as a function of c_s results in the exchange isotherm of the counterion which approaches a constant limiting value at $c_s \ll C_X$. This limiting value is equal to the equivalent concentration of the fixed charges C_X. This relationship is graphically represented in Figure 8.
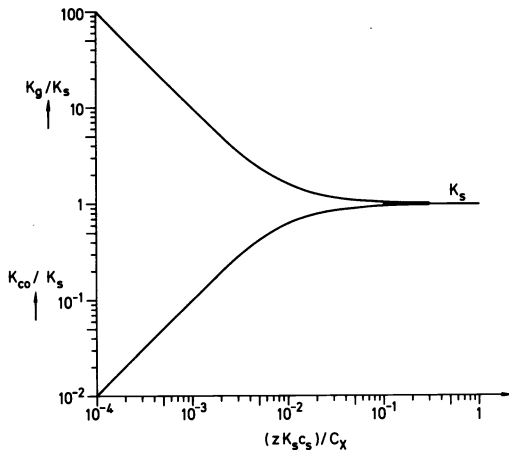

Figure 7: Calculated counter- and coion partition coefficients, K_g and K_{co}, as functions of the external electrolyte concentration c_s using a strong ion-exchange membrane [12].
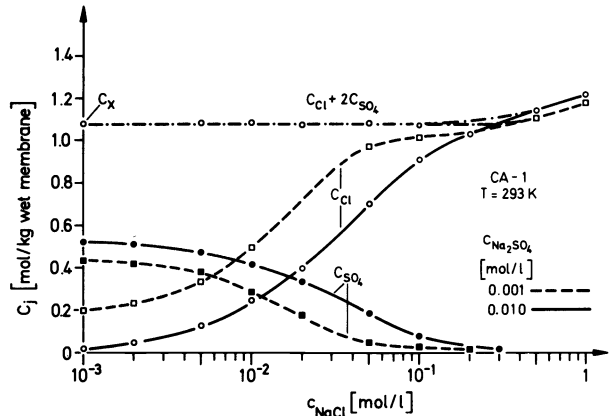
Figure 8: Experimentally established exchange isotherms as functions of the external NaCl concentration using NaCl-Na$_2$SO$_4$ solutions with different but constant Na$_2$SO$_4$ concentrations and an anion exchange membrane ASAHI A-1 at T = 25°C [13].

Determination of transport parameters

Any appropriate membrane model-independent (e.g. phenomenological, Kedem-Spiegler) and membrane model-dependent transport relationship (e.g. combined viscous-flow, solution-diffusion model, and fine-porous membrane model) can be used to evaluate the corresponding transport parameters from both suitable dialysis-osmosis and hyperfiltration data. Because of the different boundary conditions adjusted in dialysis-osmosis experiments as against hyperfiltration experiments, the transport parameters evaluated from corresponding hyperfiltration data may considerably differ from the parameters obtained from dialysis-osmosis experiments even if the same membrane sample is used. The difference in the transport parameters is especially pronounced with non-homogeneous membranes such as asymmetric or composite membranes, for instance. Moreover, applying a special model relationship in characterizing the transport properties of a synthetic membrane leads to transport parameters inherent in the underlying membrane model. Therefore, the application of just one model-dependent transport relationship will in most cases lead to one-sided statements about the membrane properties and, especially, their correlation with the membrane structure. Therefore, it is always advisable to use several different model-dependent relationships, in addition to the model-independent ones, for comparison and then look how the conclusions drawn by use of the model-dependent relationships match with the real membrane structure. On the other hand, the application of the model-independent transport relationships will always yield well defined transport parameters which, unfortunately, do not lead to a deeper insight into the physico-chemical processes governing the transport across the membrane.

Transport parameters from dialysis-osmosis experiments. Figure 9 reproduces a typical dialysis cell which can be used for the determination of transport coefficients such as the phenomenological coefficients of the linear relationships of the thermodynamics of irreversible processes which read as follows:

$$\Delta E = -r_e j + \ell_{ep}\Delta P + \ell_{e\pi}\Delta\Pi \quad (1); \quad q = \ell_{pe}j + \ell_p\Delta P + \ell_{p\pi}\Delta\Pi \quad (2); \quad \chi = \ell_{\pi e}j + \ell_{\pi p}\Delta P + \ell_{\pi}\Delta\Pi \quad (3)$$

where ΔP, $\Delta\Pi$, and ΔE are the pressure, osmotic pressure, and electrical potential difference across the membrane, respectively; ΔE must be measured with reversible electrodes such as Ag/
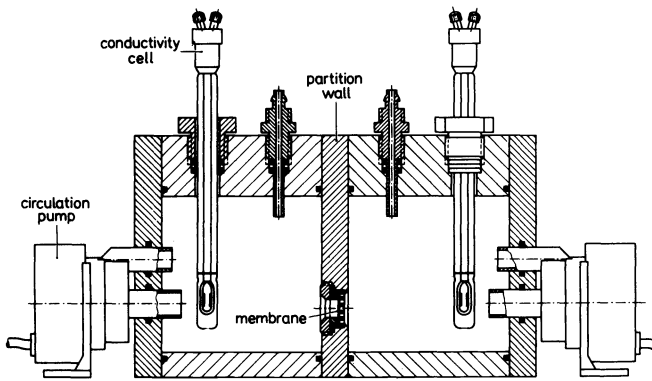
Figure 9: Exploded view of a dialysis cell [18,19]

AgCl-electrodes in the presence of Cl⁻ ions; q = volume flux {$cm^3/cm^2M \cdot s$}; j = electric current density {mA/cm^2M}; r_e = ohmic area resistance of membrane {Ωcm^2M}; $\ell_{ep} = \ell_{pe}$ = electro-osmotic permeability {$cm^3/A \cdot s$}; ℓ_p = hydrodynamic permeability of the membrane at j = 0 {$cm^3/cm^2M \cdot atm \cdot s$}; ℓ_π = osmotic permeability of the membrane at j = 0 {$cm^3/cm^2M \cdot atm \cdot s$}; $\ell_{\pi p} = \ell_{p\pi}$ = coupling coefficient at j = 0 {$cm^3/cm^2M \cdot s \cdot atm$}; $cm^2M \equiv cm^2$ wet membrane. The chemical flux, χ, is a measure of the variation of solute concentration with time within the phases adjacent to the membrane. It is related to these variations as follows:

$$\chi = (V'/A \cdot \tilde{c}_s) \cdot (dc_s'/dt) = - (V''/A \cdot \tilde{c}_s) \cdot (dc_s''/dt) \quad (4)$$

where V' and V'' are the volumes of the (')- and ('')-phase, respectively, {cm^3}; $\tilde{c}_s = (1/2)(c_s' + c_s'')$; A is the effective membrane area {cm^2M}; and dc_s/dt the variation of solute or salt concentration with time t in the corresponding compartment {phase; $mol/cm^3 s$}. In order to determine transport parameters, variations of concentrations and volumes with time in the compartments of a dialysis cell must be measured. This requires the establishment of at least a quasi-steady state. A quasi-steady state can be reached by adjusting the ratio of membrane area to compartment volume. That ratio must be chosen such that a flux across the membrane results in measurable variations of the quantities to be measured in the external solutions and concurrently does not too much disturb the formation of approximate steady-state profiles within the membrane.

In case that no electric and/or electro-osmotic transport coefficients are determined and thus no electric current across the membrane is required, transport coefficients are usually evaluated under the boundary condition of electric current being zero, j = 0. In case of that boundary condition, Equation (1) yields the electrical potential difference, ΔE, existing across the membrane:

$$\Delta E = - \ell_{ep}\Delta P - \ell_{e\pi}\Delta\Pi. \quad (1a)$$

By reason of Equation (1a), an electric potential difference generally exists across a membrane at j = 0 if pressure and/or osmotic pressure differences are present. If this electrical potential difference is measured by means of calomel electrodes with liquid junctions instead of Ag/AgCl-electrodes, for instance, it is termed membrane potential and referred to as $\Delta\varphi$ {mV}. Indeed, the linear relationship (1a) is only valid in case of small transmembrane pressure and/or concentration differences. As discussed by Schlögl [14], the membrane potential at larger concentration differences across the membrane can be calculated using appropriate integrals of the corresponding Nernst-Planck equations.

Under the usually adjusted boundary condition j = 0, the linear relationships (1) to (3) reduce, in addition to Equation (1a), to the following two transport relationships:

$$q = \ell_p\Delta P + \ell_{\pi p}\Delta\Pi; \quad \chi = \ell_{\pi p}\Delta P + \ell_\pi\Delta\Pi$$

With the definition of the reflection coefficient $\sigma \equiv -\ell_{\pi p}/\ell_p$, given by Staverman [15], Equations (2) and (3) finally yield:

$$q = \ell_p(\Delta P - \sigma\Delta\Pi) \quad (2a); \quad \chi = -\sigma\ell_p\Delta P + \ell_\pi\Delta\Pi \quad (3a)$$

All transport measurements will be affected by unstirred boundary layers. There will always exist an unstirred boundary layer at the membrane surfaces even in case of vigorous stirring of the external solutions. As schematically presented in Figure 10, concentration profiles will develop in the boundary layer yielding solute concentrations at the membrane surfaces which differ from the bulk concentrations and thus affect the effective osmotic pressure difference across the membrane, for instance. If the stirring of the external solutions is extremely effective, the deviations of the concentrations directly at the membrane surfaces from those of the bulk solutions might be comparably small and thus the effect of the concentration profiles within the boundary layer on the measured fluxes is within the error of measurement. In this limiting case, the boundary layers might be considered as part of the membrane. One has to deal with the boundary layer effects separately only in case of compa-
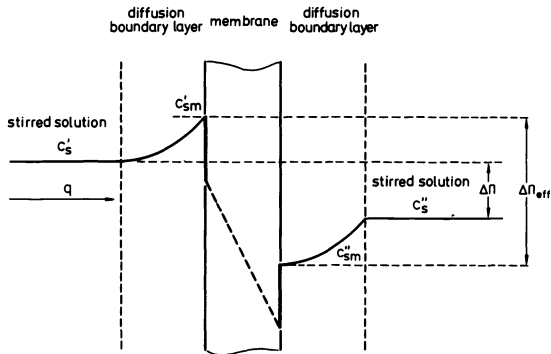
Figure 10: Diagrammatic presentation of concentration profiles within the diffusion boundary layers adhering to the membrane surfaces [18].
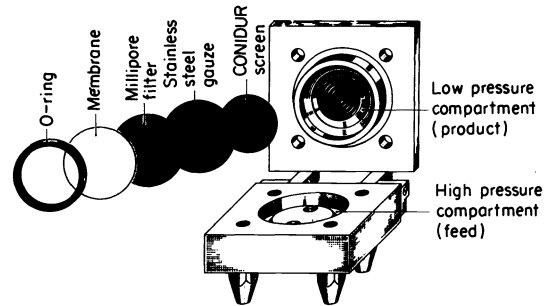
Figure 11: Exploded view of a hyperfiltration cell [18,19]

rably large membrane permeabilities. Dresner et al. [16] and Brian and Fisher [17] elaborated in detail the boundary layer effects in hyperfiltration systems for laminar and turbulent flow of the feed solution.

Transport parameters from hyperfiltration experiments. Performing permeation measurements under high hydrostatic pressure, the membrane is placed into a hyperfiltration cell as shown in Figure 11. The membrane has to be supported in order to prevent rupture at high hydrostatic pressures. The following arrangement of special supports has been proved optimum for this purpose: a CONIDUR-screen (Hein, Lehmann & Co., AG, Düsseldorf, Germany) is overlaid with a stainless steel gauze with mesh sizes from 5x5 µm to 10x10 µm. This stainless steel gauze is topped by a Millipore filter with an average pore size of 0.8 µm or even less. This arrangement provides sufficient mechanical support for the test membrane at pressures up to 100 atm or even more. The hyperfiltration cells can be arranged in series, six, for instance, and have to be located in a thermostatted water basin to maintain constant temperature in the cells [11].

The high pressure compartments of the six cells are connected in series in order to obtain the maximum possible streaming velocity of the feed solution in each cell and thus minimizing concentration polarization effects. With a gap of about 0.7 mm between the upper membrane surface and the ceiling of the high pressure compartment, a circulation velocity in the high pressure compartments from 1 m/s up to 4 m/s can be achieved. At these circulation velocities and the permeation rates of usual membranes (up to maximum 10^{-3} cm^3/cm^{2}M·s), boundary layer effects are negligible and thus no correction for concentration polarization effects has to be performed.

The feed solution is contained in a thermostatically jacketed stainless steel reservoir with a capacity of about 10 liters, and is circulated by means of a diaphragm-metering pump manufactured by Orlita (Gießen, Germany), for instance, capable of delivering up to 150 l/h. The pressure fluctuations caused by the stroke of the diaphragm metering pump are damped out by means of a 2-liter pneumatic accumulator. The gas is separated from the feed solution by a Viton-membrane within the damper. Using suitable pressure regulating valves such as RECO-mini-pressure regulators, for instance, and a corresponding PI-pressure regulating system such as INDIKON or FOXBORO, for instance, connected to a pneumatic pressure transducer, the pressure in the high pressure compartment of the hyperfiltration cells is maintained constant within ±0.05% to ±0.20%. The pressure is measured with an accuracy of ±0.1% of full scale (100 atm) using an appropriate high-pressure gauge. The feed is continuously cleaned by an in-line Millipore cartridge type filter. A skeleton sketch of the whole assembly is shown in Figure 12.
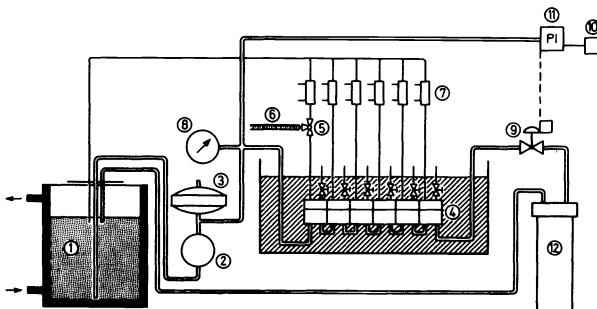

Figure 12: Skeleton sketch of hyperfiltration assembly. 1, thermostatted feed container; 2, diaphram-metering pump; 3, damper; 4, series arrangement of 6 hyperfiltration cells; 5, 3-way tap; 6, calibrated pipette; 7, through-flow conductivity cells; 8, pressure gauge; 9, pressure regulating valve; 10, pneumatic pressure transducer; 11, INDIKON pressure regulator; 12, Millipore inline-filter cartridge [19].
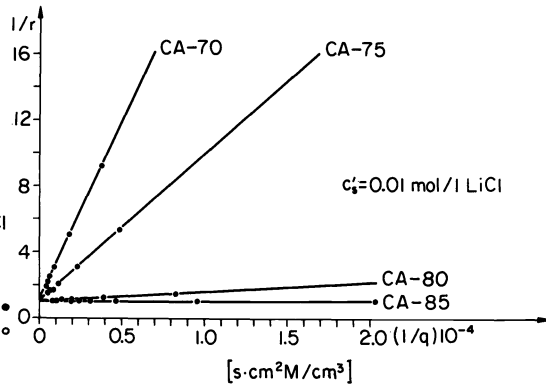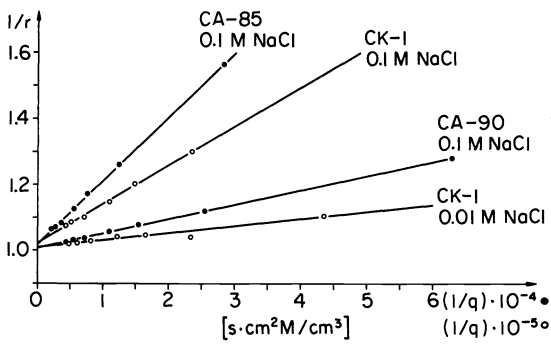
Figure 13a: Reciprocal salt rejection, 1/r, r = (c'_s − c"_s)/c'_s, as a function of reciprocal volume flux, 1/q, using 0.01 and 0.1 M NaCl brine solutions at 298 K with a cation exchange membrane (ASAHI CK-1) and asymmetric CA membranes prepared from BAYER Cellit K-700 and annealed at 85°C and 95°C. The feed pressure P' ranged from 10 to 100 atm. The points are the experimental values whereas the lines are the calculated regression lines [22].

Figure 13b: Reciprocal salt rejection, 1/r, as a function of reciprocal volume flux, 1/q, using 0.01 M LiCl brine solution at 298 K with differently annealed asymmetric CA membranes prepared from BAYER Cellit K-700 (CA-70 = annealed at 70°C). The feed pressure P' ranged from 10 to 100 atm. The points are the experimental values whereas the lines are the calculated regression lines [22].

The volume flux, q, and the solute rejection, r, are measured at the steady-state of the system which is reached when the concentrations c'_s and $c"_s$ no longer change with time. At the limiting condition of high feed concentration c'_s and low pressure differences across the membranes, the steady-state is probably approached in between two to four weeks depending on the permeation rates of the membranes used. The volume flux, q, can be measured to an accuracy of ±0.5% using calibrated capillaries such as enzyme pipettes with a calibration of 1/1000 ml.

Before the actual test measurements are performed, the membranes must be pre-pressurized at the highest pressure to be applied during the test for about three to five days using pure water as the feed solution in order to minimize compaction effects, especially for those membranes with lower water contents. After the necessary preparations, the volume flux, q, and the solute rejection, r, are determined as functions of the pressure difference, ΔP = P', at constant solute concentration of the feed solution, using the measured feed and filtrate concentrations c'_s and $c"_s$. With q and r measured as functions of the pressure difference at different but constant feed concentrations, it is then possible to evaluate the transport parameters inherent in the various transport relationships. In the case where the phenomenological relationships are applied, the three transport parameters ℓ_p, ℓ_π and $\sigma = r_\infty$ can be determined by plotting 1/r as a function of 1/q and q as a function of ΔP and calculating the corresponding regression lines which read as follows:

$$1/r = 1/r_\infty + \left((\ell_\pi/\ell_p - r_\infty^2)\cdot\ell_p\Pi'/r_\infty\right)\cdot(1/q) \quad (5a); \quad q = \ell_p(\Delta P - r_\infty\Delta\Pi) \simeq \ell_p(\Delta P - r\cdot r_\infty\Pi') \quad (5b)$$

where the approximation $\Delta\Pi \simeq r\cdot\Pi'$ has been used. First, the asymptotic solute rejection, r_∞, is obtained from the intersection of the corresponding regression line with the ordinate. Using this asymptotic solute rejection, the hydrodynamic permeability ℓ_p results from the slope of the q vs. (ΔP − r_∞ΔΠ) regression line. Therewith, ΔΠ is calculated from the measured feed and filtrate concentrations employing the corresponding osmotic coefficients:

$$\Delta\Pi = RT\cdot(\nu_+ + \nu_-)\cdot(f'_0 c' - f"_0 c")$$

where f'_0 and $f"_0$ are the osmotic coefficients of the feed solution and filtrate, respectively. After the evaluation of r_∞ and ℓ_p, ℓ_π can be calculated from the slope of the 1/r versus 1/q regression line using the osmotic pressure of the feed solution, Π'. Typical 1/r vs. 1/q plots are reproduced in Figures 13a + b.

Alternatively, utilizing the Kedem-Spiegler relationships [20] which read as follows:

$$1/(1 - r) = 1/(1 - r_\infty) - \left(r_\infty/(1 - r_\infty)\right)\cdot\exp\left[-q(1 - r_\infty)d/\varepsilon\cdot P_s\right] \quad (6a)$$

$$q = (\varepsilon\cdot P_w/d)(\Delta P - r_\infty\Delta\Pi) \quad (6b)$$

where ε designates the membrane porosity {cm^3 pore vol./cm^3M} and P_s the solute permeability {cm^2M/s}, a least-squares analysis of corresponding experimental data, r and q as functions of the feed pressure, yields the following transport parameters: $\varepsilon\cdot P_w/d$, $\varepsilon\cdot P_s/d$, and r_∞.

The following remarks are necessary regarding the determination of transport parameters for asymmetric and composite membranes as well as multilayer membranes. Performing hyperfiltration experiments with asymmetric membrane systems and evaluating the corresponding transport parameters, results, on the one hand, in the overall hydrodynamic and osmotic permeability of the asymmetric membrane system where the main part of the hydrodynamic resistance might originate from the top layer of the asymmetric membrane. On the other hand, the asymptotic rejection is completely determined by that membrane surface contacting the feed solution as demonstrated previously [21,22].

The slope of the $1/r$ versus $1/q$ line is referred to the normalized solute permeability of the membrane in the following way [18,22]:

$$\omega^* = (\ell_\pi/\ell_p - r_\infty^2)\cdot\ell_p\Pi'/r_\infty = \varepsilon\cdot P_s/r_\infty d$$

Therefore, the slopes of the $1/r$–$1/q$ straight lines are measures of the normalized solute permeabilities P_s/d of the membranes provided r_∞ does not deviate too much from the value 1 ($r_\infty \simeq 1$). Keeping in mind this correlation, a $1/r$ versus $1/q$ plot supplies an effective tool for a quick comparison of the solute permeabilities of different membranes. As is thus obvious from Figure 13a, the normalized solute permeability of the CA-85 membrane for NaCl in the presence of a 0.1 M NaCl brine solution is larger than that of the CK-1 and CA-90 membrane. On the other hand, the normalized NaCl permeability of the CK-1 membrane in the presence of a 0.01 M NaCl brine solution is much lower than its normalized permeability in case of a 0.1 M NaCl brine solution. Furthermore, the annealing effect on asymmetric CA membranes is obvious from Figure 13b. The normalized LiCl permeability decreases with increasing annealing temperature of the membrane. It should be noted that the normalized salt permeabilities of the asymmetric CA membranes for common salts will vary in a similar way with annealing temperature as the LiCl permeability although their absolute values might drastically differ.

CONCLUSIONS

A comprehensive electron microscopic investigation of synthetic membranes combined with a detailed physico-chemical characterization of their equilibrium and transport properties renders possible a clarification of the membrane structure and its organization as well as the elaboration of the transport mechanisms of solvent and solute. In addition, a comparison of the separation and transport properties of different membranes is made possible enabling the selection of membranes with optimum performance for a distinct separation process.

REFERENCES

1. W. Pusch and A. Walch, J. Membrane Sci., 10 (1982) 325, and Ang. Chem., 94 (1982) 670; IE 21 (1982) 660.
2. N. Choji, W. Pusch, M. Satoh, T.-M. Tak, and A. Tanioka, Desalination, 53 (1985) 347.
3. D.J. Ferry, Chem. Rev., 18 (1936) 373.
4. The author is obliged to Mrs. W. Schaefer and Dr. D. Dietrich, ENKA AG, Research Institute Obernburg, Germany, for the supply of the electron micrographs.
5. H.-G. Burghoff and W. Pusch, J. Appl. Polymer Sci., 20 (1976) 789.
6. H.K. Lonsdale, U. Merten, R.L. Riley, J. Appl. Polym. Sci., 9 (1965) 1341.
7. A.D. MacLaren and J.W. Rowen, J. Polymer Sci., 7 (1951) 289.
8. H.-G. Burghoff and W. Pusch, J. Appl. Polymer Sci., 23 (1979) 473.
9. H.-G. Burghoff and W. Pusch, J. Appl. Polymer Sci., 20 (1976) 789.
10. J.L. Williams, H.B. Hopfenberg, and V. Stannett, J. Macromol. Sci. Phys., B3 (1969) 711.
11. W. Lukas and W. Pusch, in: Biophysics of Water, F. Franks and Sh. Mathias, Eds., John Wiley & Sons, Chichester, 1982, pp. 27–31.
12. W. Pusch, CIT, 22 (1975) 914.
13. W. Pusch, Proc. 7th Intl. Symposium on Fresh Water from the Sea, Vol. 2, pp. 207–224, A. A. Delyannis and E.E. Delyannis, Eds., published by the editors, Athens, 1980.
14. R. Schlögl, Z. phys. Chem., N.F., 1 (1954) 305.
15. A.J. Staverman, Rev. Trav. Chim. Pays-Bas, 70 (1951) 344.
16. J.S. Johnson, Jr., L. Dresner, and K.A. Kraus, in: Principles of Desalination, K.S. Spiegler, Ed., Academic Press, New York and London, 1966, p. 383.
17. T.K. Sherwood, P.L.T. Brian, R.E. Fisher, Mass. Inst. Tech. Rept. 295-1; OSW, Res. & Develop. Progr. Rept. 95, 1964.
18. W. Pusch, Ber. Bunsenges. physik. Chem., 81 (1977) 854, und Habilitationsschrift, Johann-Wolfgang-Goethe-Universität, Frankfurt am Main, Dezember 1978.
19. W. Pusch and A. Walch, Recent Developments in Separation Science, Vol. 3, N.N. Li, Ed., CRC-Press, Cleveland, Ohio, 1978, pp. 1–12.
20. O. Kedem and K.S. Spiegler, Desalination, 1 (1966) 311.
21. S.-T. Hwang and W. Pusch, in: Synthetic Membranes, Vol. I, Desalination, A.F. Turbak, Ed., ACS Symposium Series 153, American Chemical Society, Washington, D.C., 1981, pp. 253–266.
22. W. Pusch, Desalination, in press; and in: Measurement and Control in Desalination, Ch. 1.4, N. Lior, Ed., Elsevier Publishing Corp., Amsterdam, in press.